



Monitoring, modeling, and forecasting long-term changes in coastal seawater quality due to climate change

Received: 22 August 2023

Accepted: 7 March 2025

Published online: 17 March 2025

 Check for updates

Xianghong Guan ^{1,4}, Hua Huang ^{1,4}, Xiong Ke¹, Xiaoqian Cheng¹, Heng Zhang¹, Acong Chen ¹, Guanglei Qiu ¹, Haizhen Wu² & Chaohai Wei ^{1,3} 

As climate change affects the physicochemical properties of coastal water, the resulting element re-exposure may override the emission reductions achieved by human pollution control efforts. Here, we conduct an analysis the water quality-climate effect over eight consecutive years from 2015 to 2022 along the South China coast combined with CMIP6 Scenario Model Intercomparison Project. Then we utilized a data-driven model to predict the concentrations of trace metals and nutrients over the next 80 years. It is suggested that the acidification process carries the risk of triggering the ocean's buffering mechanisms. During this alkalinity replenishment process, trace metals, such as Cd, Cr, Cu, Fe, Hg, Mn, Pb, and Zn, in the sediment are released into the water phase, along with Ca^{2+} and Mg^{2+} . Here, the aim of this study is to show that the nexus of re-exposure-eutrophication-emission reduction with human activities and climate feedback, cannot be ignored in the pursuit of effective environmental governance.

The nearshore environment is a theater of high productivity and diversity, including food supply, nutrient cycling, and organic matter mineralization. Despite covering less than 8% of the seafloor and less than 0.5% of the seawater, the coastal zone bears disproportionate marine primary productivity and becomes one of the most important carbon sinks on the Earth^{1–4}. However, this crucial water sector is suffering from potential impacts from climate change. Acidification leads to changes in the phase distribution of trace metals (TMs, Cd, Cr, Cu, Fe, Hg, Mn, Pb and Zn), affects the functions of electron donors involved in cell respiration, and disrupts enzymatic reactions⁵. In addition, the increase in H^+ concentrations caused by ocean acidification alters the chemical form of metals, thus affecting their toxicity and bioavailability in seawater⁶. Eutrophic marine ecosystems may enhance primary productivity due to warming but weaken ecological stability⁷. The excessive inflow of nutrients and TMs affect the ecological resilience of the coastal zone. Ecosystems that have their resilience weakened will be more vulnerable to environmental changes^{8–10}.

After experiencing the period when various countries attached great importance to governance and passed the period with the largest emissions, the recycling and redistribution of elements caused by climate change may gradually replace the direct discharge from human activities and become a new pollution risk¹¹. We expect future marine ecology to be exposed to oceans with high water temperatures, uncertain rainfall fluxes, and acidification atmospheres (a result of the elevation in the partial pressure of CO_2). Due to the lower baseline concentration, TMs may become sensitive potential risks in response to changes in marine water quality. The phenomenon of eutrophication and the alteration in the coupling ratio of nutrient elements has resulted in the modification of the biogeochemical cycle in coastal areas. These aforementioned factors can potentially trigger an irreversible effect, leading to changes in the quality of coastal water.

Literature statistics based on meta-analysis¹² show that the current research focus in the field of inshore waters under climate change primarily revolves around hydrological characteristics, including sea

¹School of Environment and Energy, South China University of Technology, Guangzhou 510006, P. R. China. ²School of Biology and Biological Engineering, South China University of Technology, Guangzhou 510006, P. R. China. ³School of Environment and Energy, Guangdong Provincial Key Laboratory of Solid Wastes Pollution Control and Recycling, South China University of Technology, Guangzhou 510006, P. R. China. ⁴These authors contributed equally: Xianghong Guan, Hua Huang. ✉e-mail: cechwei@scut.edu.cn

level, ocean currents, tides, and environmental indicators. Element migration encompasses various processes, such as the interaction between the earth and water, the interaction between gas and water, and the diffusion of salt and TMs resulting from the confluence of river and ocean currents. Sea surface temperature (SST)¹³, rainfall^{14,15} and partial pressure of carbon dioxide ($p\text{CO}_2$)¹⁶ are considered to be influencing factors of these transmission routes:

Sea surface temperature affects the phase distribution of elements from biological and chemical aspects. In the exchange of the earth-water interface, the processes of bio-utilization, release, circulation, and remineralization of C, N, P, and S elements lead to the movement of metal elements into the dissolved phase¹⁷. Sea surface temperature also affects the suspension of metal elements caused by biological action¹⁸. Additionally, changes in sea surface temperature influence dissolved oxygen levels, altering the redox potential of the solution as a whole and affecting the hydrophilicity of elemental compounds. Consequently, these intertwined physical-chemical-biological effects affect the water/sediment phase equilibrium¹⁹.

In the exchange at the air-water interface, atmospheric deposition is the primary pathway for land-based nutrients, such as N and S²⁰. Incompatible elements have a larger radius, low melting and boiling points, such as Hg, Cd, and Pb, also enter the ocean through this process. With the advancement of society, wet deposition, which mainly carries nitrate, has become the chief N input pathway to the coastal areas²¹. Nitrogen deposition has become one of the factors behind the coastal eutrophication²². The accounting of mercury's cross-media flux shows that, for the modern open ocean, the dry and wet deposition flux of Hg(II) is 4600 mg yr^{-1} , the uptake of Hg(O) is 1700 mg yr^{-1} , and the confluence of rivers is $2050\text{--}5600 \text{ mg yr}^{-1}$ ²³, which reflects that the process of sea-land subsidence is the main source of marine Hg.

As the concentration of atmospheric carbon dioxide increases, the acidity of the ocean grows rapidly. During eutrophication, biogeochemical feedback further increases the supply of N and P, and if there is sufficient N input, estuarine and coastal marine ecosystems can be driven to P limitation. This conversion leads to greater far-field N pollution, pushing eutrophication over greater distances. The physical oceanography of coastal systems (degree of stratification, residence time, etc.) determines their sensitivity to hypoxia²⁴. The metals in the acid-soluble and reducible fractions migrate in response to the variation of marine water quality²⁵. The stratification of ocean temperature and density modifies the nutrient transport²⁶. Consequently, both nutrients and trace metals (TMs) can further influence the open sea via ocean currents. Due to the difference between terrestrial and marine water bodies, the input ratio will have a notable impact on the pH of the aqueous solution. Obviously, the above three factors (sea surface temperature, atmospheric deposition, and pH) not only affect the exchange of elements but also respond to climate change, which will become the model variable to predict the cycle of elements under climate change.

Although there is sufficient evidence to prove the notable impact of the physico-chemical properties of seawater solution on the tendency of elemental migration, the combined effect of influencing factors in future situations is still unknown. It is unclear whether the tendency of elemental migration in specific areas, under the framework of climate warming, rainfall change, and ocean acidification, creates new environmental risk points. Therefore, representative datasets and reliable prior models are needed to monitor and simulate long-term changes in sea areas. This paper focuses on data over eight years (2015 to 2022) of South China, which located along the South China Sea, has a coastline of 4114.3 km, the longest coastline in China²⁷. The region includes the Pearl River, the 18th largest river in the world with a flow rate of $207 \times 10^9 \text{ m}^3 \text{ yr}^{-1}$, as well as 52 medium-sized rivers with catchment areas exceeding 1000 km² and 614 small streams. The sea area is influenced by the Kuroshio warm current and the coastal

current of the South China Sea. The climate is controlled by several subsystems, including the Pacific Ocean, Indian Ocean, and Eurasian Continent. Additionally, it has experienced the impact of the super El Niño from 2015 to 2016 and La Niña from 2020 to 2022. These extreme global hot and cold events cause significant fluctuations in Sea Surface Temperature (SST), dry and wet deposition, and surface runoff. As a result, the variable range of the model becomes wider, which is beneficial to simulate future thermal events. To accurately model these fluctuations, we intend to establish a ternary receptor model with background values. This model will consider the influence of three factors, including sea surface temperature, dry and wet deposition amount, and pH, on the migration tendencies of different elements. Its reliability was tested by conducting stability and heterogeneity analyses using meta-analysis. Moreover, the model was compared with machine learning methods to evaluate its accuracy. Once a reliable receptor model had been established, the Climate Model Inter-comparison Project 6 (CMIP6) version of the CanESM5 model was employed to predict the future water quality. The long-term concentration variation and trend of nutrients and TMs in the coastal zone for the next 80 years were calculated and discussed based on the physico-chemical properties of seawater. The data of three variables output by the experiment ID of SSP3-7.0 were used to fit the measured data, and a receptor model was constructed to predict nutrients and TMs. SSP3-7.0 represents a moderate warming rate close to the actual, temperatures are projected to rise by 2.7 °C. Simultaneously, the partial pressure of carbon dioxide is expected to increase by two-thirds by the end of the century, resulting in significant changes in the oceanic element cycle. Developing a twin model that accurately reflects the response of water pollution to changes in water quality offers an opportunity to quantify the inevitable secondary risks posed by climate change. It reveals the pollution exposure risks of the increasingly acidified oceans, especially in the estuarine environment with high nutrient concentrations and increasing carbon dioxide partial pressures.

Results and discussion

Spatial and temporal variations in datasets

In the case of short-term environmental changes, despite the existence of large spatial differences, the implementation of environmental protection policies has stabilized the overall trend of water quality in the studied area. There are notable differences in the concentration and dispersion of TMs in the coastal waters of Guangdong Province. This allows our model's dependent variables to respond sensitively to parameters and reflect a wide range of spatiotemporal variations. The average annual concentrations of nine TMs in the three urban agglomerations do not exceed the limits of National Recommended Water Quality Criteria²⁸. This suggests that the surveyed area represents a typical scenario of the continental shelf seas of the Anthropocene, which have maintained normal ecological functions despite notable disturbances by human activity. The concentration of TMs varies greatly among urban agglomerations, influenced by the economic and industrial structure, scale of cities, and the unique hydrological environment. Based on the standardized systematic clustering results of cross sections (Supplementary Table 1) and the local natural conditions and economic layout of the Guangdong Province, this paper divides the studied area into three sub-areas. This means that the fitting process needs to provide three geochemical background values, including Pearl River Delta (PRD), East Coast, and West Coast.

The per capita Gross Domestic Product (GDP) of the region in 2022 had reached 14,557 USD, which places it at the inflection point of the environmental Kuznets curve for metal elements. This means that metal consumption is undergoing a transition from a sharp increase to a stable trend, and the subsequent pollution activities are being stabilized and improved through cleaner production and terminal treatment¹¹. Specifically, the concentrations of Cd, Cr(VI), and Hg in the

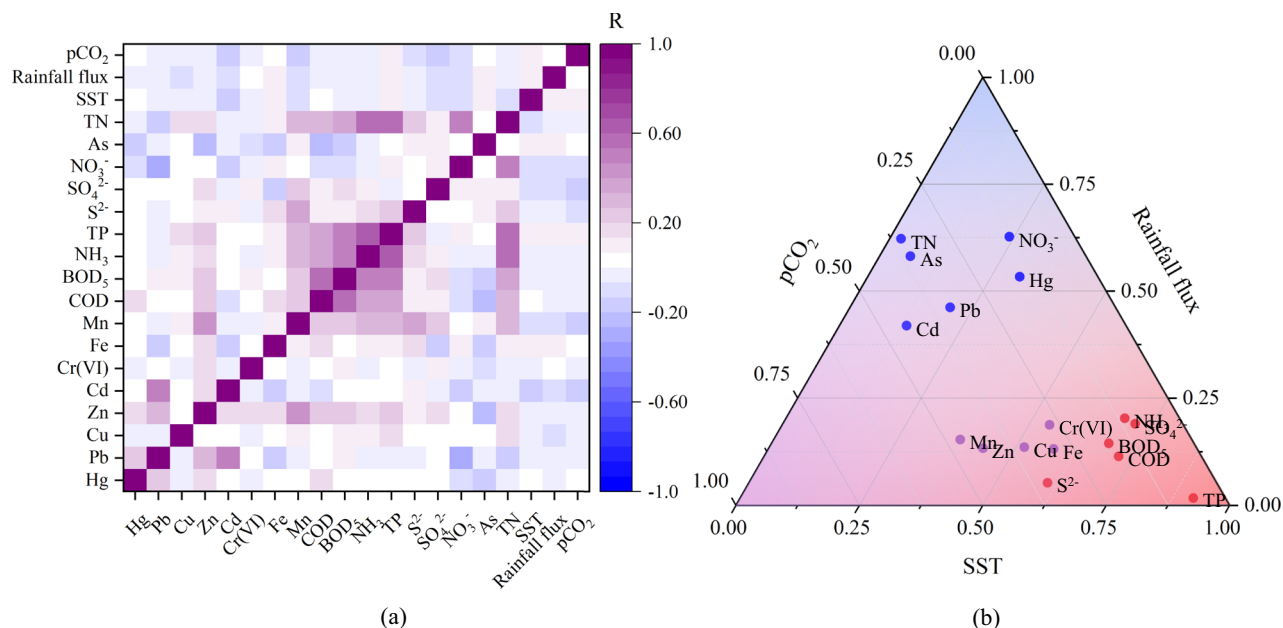


Fig. 1 | The correlation of indicators and the sensitivity of pollutant species to environmental variables are presented in (a) and (b) respectively. a The correlation of each index to these three variables. Double correlation analysis of key response factors of climate change and elements in coastal water bodies. Positive correlations are indicated by purple, while negative correlations by blue. The intensity or darkness of the color represents the strength of the correlation, with darker colors signaling a stronger correlation; **(b)** The feature importance of each

index to these three variables. It depends on the use, chemical properties, and migration trend of the elements. According to the difference in response to variables, elements are divided into three categories, in which red represents sea surface temperature (SST)-sensitive elements, blue represents sedimentary-sensitive elements, and purple represents elements that play multiple roles in the geochemical process.

urban agglomerations of the east and west coasts show an overall decreasing trend. However, the urban agglomerations of the PRD exhibit a peak-shaped trend, reaching an inflection point in 2019. One possible factor contributing to the change in Hg deposition in the Pearl River Delta region is the reduction in cement production²⁹. Another notable source of TMs is coal and petroleum combustion. Attributes to the addition or upgrade of air pollution control devices for combustion sources in recent years, the capture of TMs has become more effective³⁰. The contribution of the coal industry is relatively low due to the high removal rate of Pb and Cd.

Meanwhile, total nitrogen (TN) and $\text{NH}_3\text{-N}$ pollution in the core urban agglomeration of the PRD and along the coast of western Guangdong Province reached its peak concentration in 2017–2018, exceeding the local water quality standard limit of 1 mg L^{-1} . The overall five-day biochemical oxygen demand (BOD_5) and total phosphorus (TP) pollution have shown a downward trend. Nitrogen is the main limiting nutrient in the PRD region, primarily entering coastal waters through the sea and land. Rivers play a notable role in transporting nutrients, with freshwater culture contributing a staggering 20% (N) and 53% (P) of compounds³¹. In the environment of ocean acidification, active phosphorus will be released from the sediments into water³², while eutrophication and weak acid-base buffering capacity will enhance anthropogenic CO_2 -induced acidification³³. Under strict control measures, the concentration of nutrients in the surface layer of the ocean remains stable.

With the continuation of strict environmental protection policies and the improvement of cleaner production practices, it is evident that most pollution indicators exhibit a stable or declining trend, as predicted by the environmental Kuznets curve, that is, the concentration of pollutants in the region has reached its maximum value. Have efforts to reduce emissions of TMs and nutrients ensured that these pollutants no longer cause significant pollution events? Still, it is important to acknowledge that the dissolution and mineralization of TMs and nutrients is influenced by natural factors such as temperature and

REDOX potential. The alteration of phase partitioning, brought about by climate change, is a matter that demands our attention. It is crucial to commence by examining the physico-chemical properties of sea-water solutions and subsequently forecast the future water quality.

Key factors in the interactions of aqueous solution properties (ASPs) in the nearshore environment

There are multicollinearity between factors (Fig. 1a), such as the correlation between human activities and CO_2 concentration, and the correlation between SST and eutrophication. This allows us to describe the variation of elemental compounds with a small number of factors. In order to identify the main factors in the complex interaction among the ASPs in the nearshore environment, Principal Component Analysis (PCA) was carried out. The three components, which correspondingly are SST, deposition, and pCO_2 , contributed 28.9%, 15.3%, and 13.9% of the variance, respectively (Supplementary Table 9). The identification of the three main components is described in **Part C of the Supplementary Information**.

The receptor model is constructed based on the following principles. (I) Each of the three subareas has a geochemical background value, which is identified as the initial value of the forecast model. The geochemical background values have been affected by continuous human activities in the Anthropocene era, and this disturbance activity is assumed to be stable. (II) As this is a prediction model for studying the long-term evolution of concentration, only the macro mechanism is discussed. The three variables, SST, deposition, and pH, essentially refer to the exchange between water-biofacies/sedimentary phase, water-vapor phase, and land-marine input. Although the intermediate mechanism is very complex, a linear model is used to describe the effects of these three aspects. (III) The changes in the dependent variables of the dataset are assumed to follow a normal distribution, and they are influenced by concentration peaks produced by the three independent variables. Regression fitting of TMs and nutrient compounds was carried out based on the measured results from 2015 to

2021 and the corresponding variable data. (IV) The values of the three sections are fitted with their respective geochemical background values, and the median value of the peak with the largest sample size should be extracted using the box diagram method.

Here, a decomposition of the total amount of elemental fluctuations (total variance) from the composite factors was achieved, based on the average of the indicators, and the weights affected by SST, deposition, and $p\text{CO}_2$ were calculated. The results obtained are represented by a triangle diagram (Fig. 1b). Ingredients can be divided into three categories based on their different responses to variables. In the sensitivity analysis, the elements with sensitivity coefficient greater than 0.25 are identified as sensitive elements, and they show sensitive response behavior to specific variables.

(1) Elements sensitive to SST, such as small molecules generated through respiration and components that require biological activity intake, including BOD_5 , chemical oxygen demand (COD), S^{2-} , SO_4^{2-} , and so on. $\text{NH}_3\text{-N}$ and TP are also included, but they are also sensitive to the acidification process.

(2) As for elements sensitive to rainfall flux, namely Cd, Hg, and Pb, rainfall is an important way for them to enter the offshore area³⁴.

(3) The elements at the center of the triangle: Fe, Cu, Mn, Zn, etc., play multiple roles in geochemical processes. These include: electron donors (affected by $p\text{CO}_2$), nutrients (affected by SST), ligands (affected by $p\text{CO}_2$), as well as acid deposition and weathering and deposition in the ocean.

The behavior of the three variables (sea surface temperature, rainfall, and $p\text{CO}_2$) in the migration process of TMs depends on the exchange of elements between the ocean, atmosphere, sediments, and rivers. Direct human emissions have such an impact that different emission sources lead to high-throughput exposure to specific elements. However, the influence of the change of physical conditions of the water body is different, and the sensitive response of elements to specific factors leads to the overall change of the group of elements with similar chemical properties. As a result, the future ecological pollution pattern may be reflected in the imbalance of the coupling ratio of element groups. This means that an unhealthy mix of carbon sources (used to form carbon in microbial cells and metabolites), nutrients, TMs, salts, and other component groups can interfere with the normal biogeochemical cycle.

Discussion on the robustness and accuracy of the model

The reliability test of the model needs to be completed by discussing the sensitivity and robustness of the variables. Sensitivity analysis is an effective tool for determining the relationship between two nonlinear variables. Sensitivity values greater than 0.25 indicate significant feedback effects. To enhance the robustness and explanatory power of the indicators, parallel variables were used as controls, including dissolved oxygen concentrations, wet and dry deposition, and pH. The results (**Part D of the Supplementary Information**) show that the response sensitivity of other elements to the variables is greater than 0.25. After fitting, except for Mn (0.370), Cu (0.369), $\text{NH}_3\text{-N}$ (0.357), S^{2-} (0.156), and SO_4^{2-} (0.323), the R^2 of other components ranged exceeds 0.450 (**Part C of the Supplementary Information**), reflecting the low effect value of components influenced by the model on complex factors, but the overall convergence was significant ($p < 0.01$). Figure 2 reflects the relationship between measured and simulated values for different components, simulating the interannual and monthly changes well.

Machine learning models, specifically random forest and XGBoost models, perform better than traditional receptor models in fitting data sequences. However, for long-term marine environmental change simulation, the CMIP6 model's future dataset is required, which can only be linked to the receptor model. Nonetheless, the machine learning model can serve as a control group to assess the receptor model's reliability and the degree of information loss.

The recognition results of the two machine learning models in **Part D of the Supplementary Information** also support SST, rainfall flux, and $p\text{CO}_2$ as the three important variables. Compared to the random forest and XGboost model, the receptor model shows a weak fit for sulfides and sulfates. Therefore, the prediction results for these substances are not discussed in this paper. In terms of fitting R^2 for TMs, the receptor model slightly underperforms the random forest model for Cd, Cr, Cu, Fe, and Mn. However, the receptor model outperforms the random forest and XGboost model for BOD_5 and COD, as reflected by higher R^2 values. This suggests that the receptor model is better at accurately describing data when it follows a normal distribution. When the Mean Squared Error and Mean Absolute Error are compared, there is no significant difference between the two models.

Long-term changes in TMs

The process of ocean acidification depletes the alkalinity of the water column and triggers the buffering mechanism of the ocean. This leads to the exchange of seawater with minerals on the seafloor, which regulates acidity and alkalinity. Acid dissolution results in a significant release of Ca^{2+} and Mg^{2+} from the sedimentary phase into the water. However, Ca^{2+} and Mg^{2+} are compatible elements with small radii and low water solubility. Their substitution also occurs in other ions of elements with similar chemical properties, such as Fe, Mg, Cr, Cu, Zn, and so on. Based on our estimates (Fig. 3), the concentrations of dissolved Cu, Fe, Pb, Cu, Zn and Fe in 2099 will increase by $186.3\% \pm 90.9\%$, $58.0\% \pm 29.9\%$, $110.0\% \pm 102.6\%$, and $107.0\% \pm 67.3\%$, respectively, comparing to 2020. The outcome depends on the feature importance of component concentration to $p\text{CO}_2$ (Fig. 1b). The differences in simulation variables among grids have led to huge discrepancies (Fig. 4). Hg and Cd have a relatively large proportion of atmospheric sources. The uncertainty of rainfall has resulted in no significant differences in the simulation results ($-4.9\% \pm 9.0\%$ and $0.3\% \pm 3.7\%$). Mn and Cr(VI) are sensitive to the oxidation-reduction potential (ORP) of water bodies and involve complex oxidation-reduction reaction processes. The simulation results show a significant decrease ($-50.5\% \pm 46.4\%$ and $-16.1\% \pm 17.4\%$). The growth trend appears to be linear, although it may be influenced by other unexpected factors. It is important to note that our results may slightly overestimate the actual concentration due to the mutual control and the constraint mechanism among the components of natural water bodies. Previous studies have suggested that sulfides may interfere with the redissolution of TMs in low ORP water in the future³⁵. However, possibly due to the limitations of the dataset, we were unable to generalize the constraint relationship between sulfides and various TMs ($p > 0.05$), indicating that we cannot include the interference of sulfur in the receptor model. In addition, the presence of concentration levers in ion exchange process needs to be treated with caution. That is, when alkalinity is released from sediments to the aqueous phase, TMs with a lower water/sediment partition coefficient have a higher migration probability. This conclusion is derived from observation of the experimental dataset and cannot be clearly shown in the simulation results. Specifically, the cations that are deposited are abundant elements, while the relative concentration fluctuation rate in dissolved TMs is much larger compared to the Ca^{2+} and Mg^{2+} .

TMs undergo internal transformations like retention, recycling, and remineralization, contributing to their biogeochemical cycling. Biota in the surface ocean retain TMs based on their specific needs and fate, such as viral lysis, senescence, grazing, or export to depth. Rapid recycling of TMs in the surface ocean sustains higher metal bioavailability, extending their seasonal productivity¹⁷. The compatible elements (with higher melting and boiling points), such as Fe, Mn, Cu, and Zn, are primarily complexed with a higher level of COD during winter, resulting in a higher concentration in the water phase. In spring and summer, these elements are utilized by organisms through

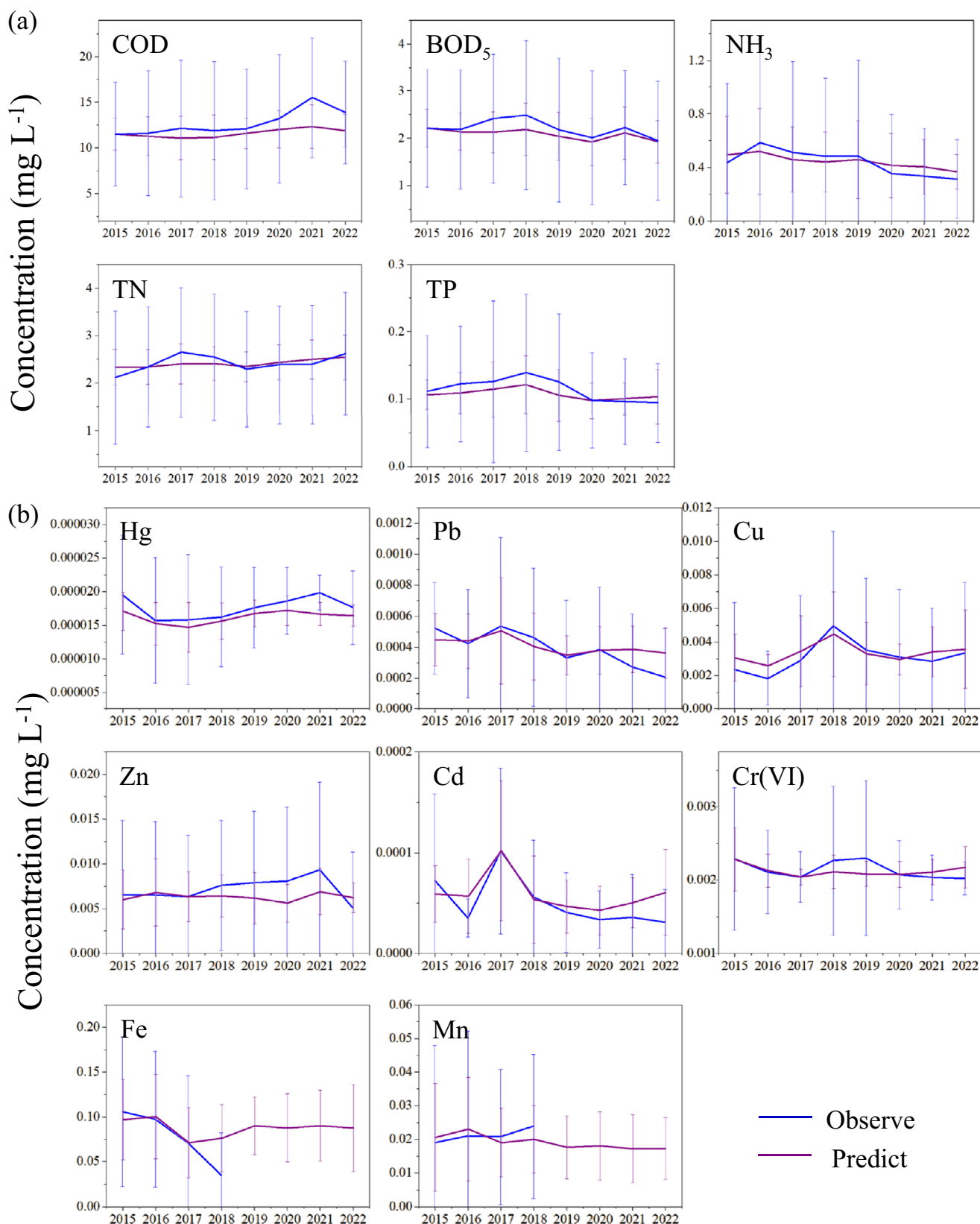


Fig. 2 | Trends in simulated results (blue line) and measured values (purple line) of the receptor model (2015–2022). Error bars represent parallel samples of multiple sampling points. **a** Represents nutrients, and part **(b)** represents trace metals (TMs).

phagocytosis or active transport, leading to a decrease in concentration. In autumn, they are mineralized or recycled into the water through organism apoptosis. In Fig. 4, the annual ranges ($R = \frac{C_{\max} - C_{\min}}{C_{\text{avg}}}$) of Fe, Mn, Cu, and Zn decreased by $40.1\% \pm 27.1\%$,

$30.1\% \pm 73.7\%$, and $106.0\% \pm 50.6\%$, respectively, suggesting a potential relationship with the decreased efficiency of the metal carbon pump under the conditions of warming and high partial pressure of carbon dioxide ($p\text{CO}_2$). This phenomenon needs to be further verified by

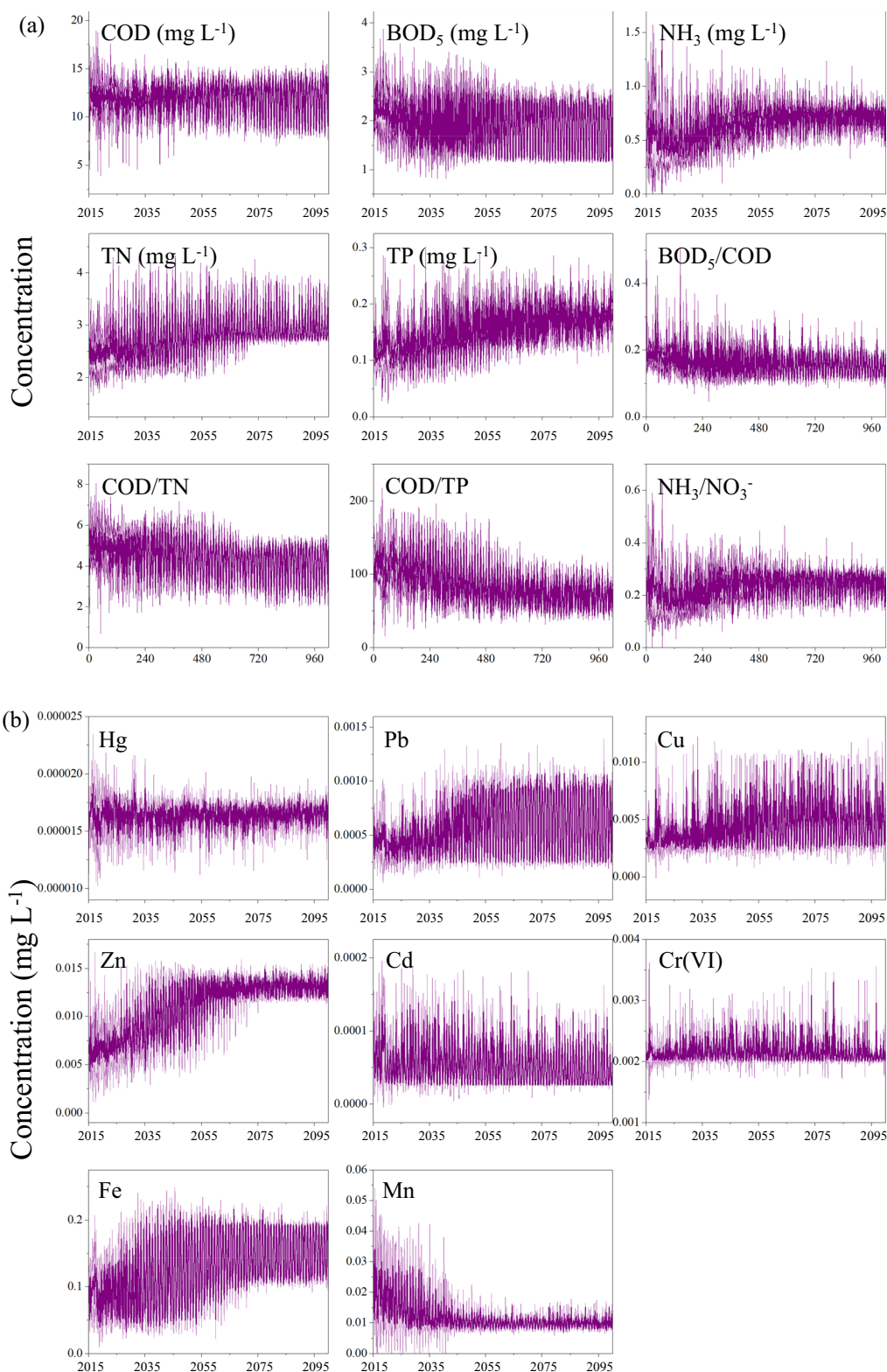


Fig. 3 | The trend of dissolved phase concentration of some water quality indices in 2015–2099. Error bars represent parallel samples of multiple sampling points. **a** Represents the changes in biological elements and their ratios, and **(b)** represents the TMs.

longer-term observational data. For the incompatible elements (with lower melting and boiling points), the ternary diagram in Fig. 1 shows the significant differences in Hg and Cd are noticeably influenced by the rainy and dry seasons. Cr(VI) is significantly affected by the sea surface temperature (SST), while the difference in its annual range is not significant. The unexpected expansion of the annual range of Pb

proves that it may be a sensitive element responding to changes in water quality.

Declining nitrogen removal performance

By means of the ratio of BOD₅ to COD (B/C), the ratio of COD to total nitrogen (C/N), and the ratio of ammonia to nitrate (NH₃/NO₃⁻), we can

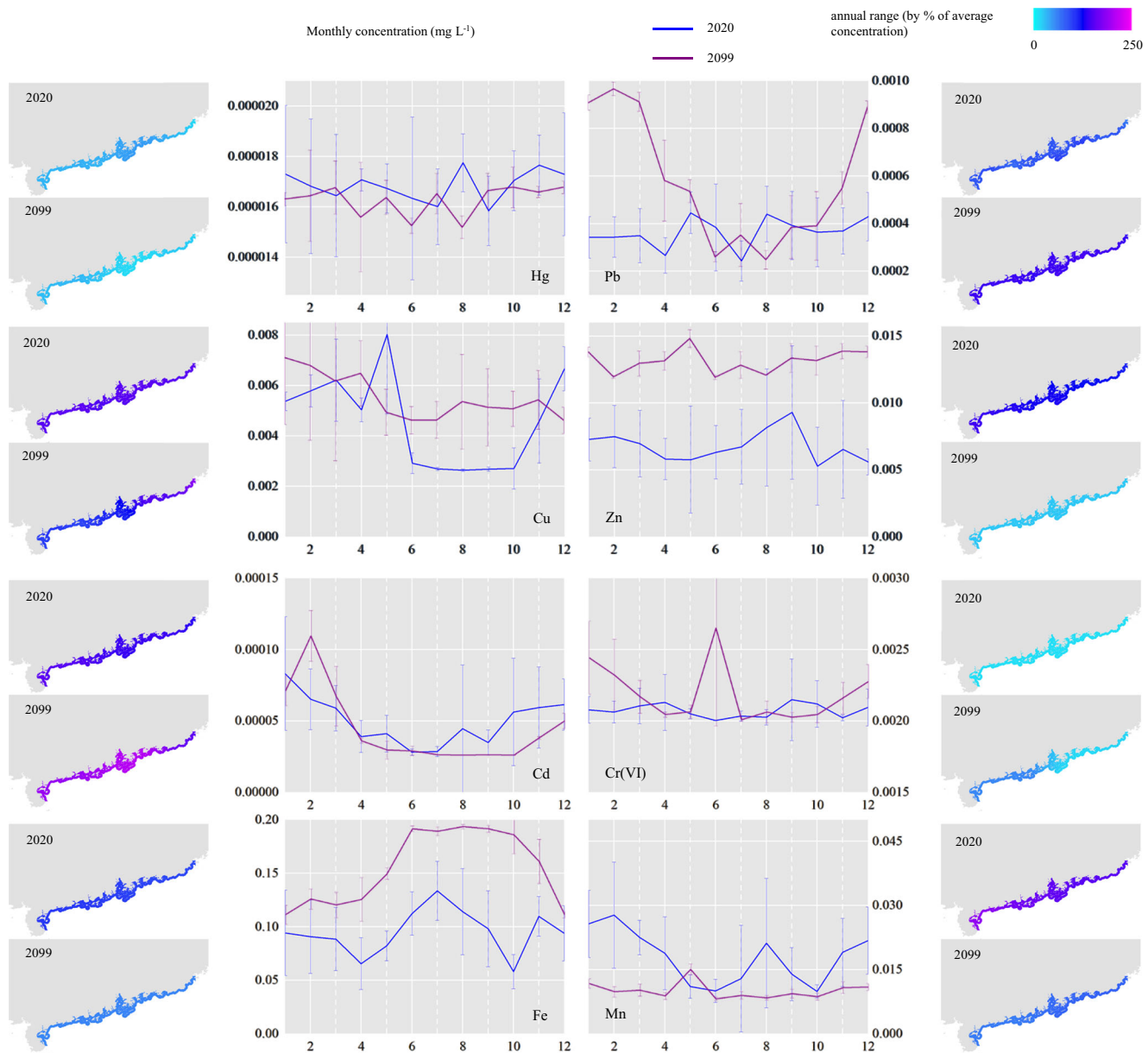


Fig. 4 | The monthly variation of metal concentrations in the aqueous phase of the study area. The annual range of concentrations represents the ratio of the difference between the maximum and minimum months to the annual average concentration ($R = \frac{C_{\max} - C_{\min}}{C_{\text{avg}}}$).

evaluate the nitrogen removal performance of a natural or engineered system^{35,36}. Our simulations found that the B/C ratio exhibits a trend of oscillating decline, and Monte Carlo simulations found that the probability of an increase of more than 1% and less than -1% was 13.1% and 35.2%, respectively. The decrease of ORP caused by the decrease of dissolved oxygen has no significant effect on B/C. The C/N ratio decreased from 5.22 ± 0.53 in 2020 s to 4.92 ± 0.91 in 2090 s, and the decrease of carbon sources may interfere with the process of nitrogen removal in the ocean. The previous experimental simulation demonstrated that the compound effect on C/N affects the efficiency of the biological pump³⁷. In addition, the proportion of $\text{NH}_3/\text{NO}_3^-$ has increased by $18.8\% \pm 4.5\%$. In the context of continuous ocean reduction and acidification, the microbially mediated reoxidation and reduction of nitrogen is inhibited, which not only includes the decrease of nitrification and denitrification rate, but also may generate additional greenhouse gas N_2O ³⁸. Another eutrophication element, phosphorus (in terms of TP), was evaluated, and it was found that it increased by $61.9\% \pm 17.3\%$ over 80 years, again indicating a

continuing decline in the coastal capacity to remove nitrogen and phosphorus.

Although some mechanistic and kinetic models link aspects of elemental cycling behavior to physical conditions, considerable uncertainty remains about the physical mechanisms, driving such changes on decadal to centennial scales. In particular, the effect of hydrological changes caused by climate change on the behavior of TMs has not been taken into account in our model. The current lack of adequately resolved and well-distributed marine proxy data for high temperature and high CO_2 scenarios prevents rigorous testing of the main factors that modulate element cycling. More advanced machine learning models cannot be applied to future simulations. Additional work is required to establish the boundary conditions and possible mechanisms (for example, the inflection point of nonlinear change of TMs in the acidification process). However, we are able to get a glimpse of the dramatic changes in the cycle of elements brought about by changes in the physical environment. We are able to further analyze and foresee the significant changes in element cycles brought about by

physical environmental changes within a regional dataset. In the context of hypoxia and acidification, the changes in the valence bonds and ion binding modes of trace metals (TMs) will lead to irreversible changes in their phase partition coefficients. The nitrification reaction caused by eutrophication consumes the alkalinity of the water body and enhances the above effect. The increase in the exposure of metal elements in the nearshore aqueous phase is comprehensive and irreversible. Marine organisms may have to survive in an environment with high concentrations of electron donors, low carbon sources, and high nutrient loads. Their growth will be affected by elevated sea temperatures, and the ecological value and sink capacity of the ocean will be irreversibly weakened.

Methods

The supporting content and data for the following four sub-items can be found in Part A, Part B, Part C, and Part D of the Supplementary Information.

Datasets on concentrations and solution conditions of elemental compounds

The pollution records of sea-entry rivers from 41 water quality monitoring stations in the coastal city cluster of Guangdong Province, South China, for the period 2015–2022 were collected (Supplementary Fig. 1 with the coordinates provided in Supplementary Table 1), and obtained from the information disclosure platform of the department of ecology and environment of Guangdong Province³⁹. The data selection process involved 2549 existing samples, which geographically covered the monitoring sections of the main rivers entering the sea in the province. In terms of time, due to the significant seasonal differences in nutrients and TMs, the sampling frequency was one month. Each dataset included water quality parameters such as pH, electrical conductivity, and DO, the concentrations of TMs like Cd, Cr(VI), Cu, Hg, Fe, Mn, Pb, and Zn, and the concentrations of non-metallic pollutants such as COD, BOD₅, NH₃-N, TN, and TP. The effective sample number (Supplementary Table 2) and frequency distribution (Supplementary Fig. 2) of each index are provided. Data on the administrative divisions and river systems of Guangdong Province, Hong Kong SAR, and Macao SAR were obtained from the geographic data publicly released by the Ministry of Natural Resources of China (<https://www.webmap.cn/main.do?method=index>).

Aqueous solution properties (ASPs) data set for modeling

CMIP6 is a project initiated under the World Climate Research Program to compare coupled models and enhance our understanding of the Earth's climate system⁴⁰. Its goal is to promote model development and facilitate scientific research by openly providing multi-model output in a standardized format. Here we use ScenarioMIP simulations from the Earth System model CanESM5. The model has a spatial resolution of 1 degrees latitude by 1 degrees longitude, and we use the monthly output from the “r1i1p1f1”. The climate change model is set as ssp3-7.0. To extract data from the model from 2015–2099, R-based `ncdf4` and raster toolkits were used. The variables include sea surface temperature, rainfall flux, and abiotic surface aqueous partial pressure of CO₂ (*p*CO₂). By using a receptor model and machine learning techniques, the changes in nutrients and TMs levels in the water area over the next 85 years were simulated and predicted. By analyzing the extracted variables, the trend of monthly change in the concentration of nutrients and TMs by the end of this century could be projected. The parameters and output results of the model can be found in the “Source Data File”.

Establishment of prediction model

To identify the main factors involved in the complex interaction between ASPs in the inshore environment, PCA was conducted. Before reducing the data dimensionality, the Kaiser-Meyer-Olkin (KMO)

sampling adequacy measure and Bartlett sphericity test were performed to detect correlations and partial correlations between variables, as well as to determine their independence. After testing, the KMO test coefficient was found to be greater than 0.5, and the significance probability of Bartlett's test (*p*) was found to be less than 0.05, indicating that PCA was suitable for conducting factor analysis on the dataset.

The behavior of pollutants in the nearshore environment is highly uncertain. Through PCA, data dimensionality can be reduced, which facilitates the identification of potential correlations or clusters among variables within the entire system, and the determination of key factors involved in the regression process of elements within this complex system. In the PCA, such tracers were selected that exhibited a strong positive or negative correlation with a single component (load > 0.8 or < -0.8), while not demonstrating a significant correlation with other component variables. In order to provide a more specific representation of solution properties, priority was given to physicochemical indices as tracer dimensions over concentration indices.

The tracer obtained from the above steps will be used as a variable in the receptor model. The number of variables depends on the number of principal components that explain the variance. In order to prevent over-fitting, the simplicity and efficiency of the model are improved. When the total variance of interpretation is greater than 0.6, the analysis of components is stopped. The tracer obtained is combined with the background value into a polynomial that describes the real-time concentrations of various components of the water body. The specific formula is as follows:

$$[\text{Concentration}] = \{A\} \times [\text{Tracer}_1] + \{B\} \times [\text{Tracer}_2] + \{C\} \times [\text{Tracer}_3] + [\text{Background}] \quad (1)$$

All variables in the above formula are unified as mg L⁻¹.

Validation of predictive models

Meta-analysis was conducted to determine the applicability of the dataset to the scenario discussed in this study. On one hand, the dataset should reflect regional spatiotemporal differences and avoid accidental coincidences resulting from random sampling. On the other hand, publication bias can significantly skew the final results of the dataset analysis, so it is necessary to implement a recognition program to eliminate any offset values. These two tests restrict the distribution range of the dataset, considering both dispersion and convergence, and heterogeneity and bias can be assessed using forest plots and funnel plots, respectively.

Heterogeneity and bias were assessed using the Meta package in the R language. Initially, the dataset was exported to a CSV file, with the concentration data assigned to the experimental group and the average to the control group. Subsequently, the Meta package was executed in R 4.3.0, and the experimental outcomes were generated following the instructions for forest and funnel plots. The forest plot output included the measurement of heterogeneity through *I*². If *I*² exceeded 50%, it indicated strong heterogeneity, implying a significant difference. Additionally, a *p* value below 0.01 denoted that the test of heterogeneity fell within a 99% confidence interval. The funnel plot was used to detect sample bias, with excessive or insufficient odds ratios suggesting biased samples. In other words, samples falling outside the inverted triangle were deemed biased. In contrast to other studies that focused on single effects through meta-analysis, our study aimed to obtain a dataset encompassing complex effects. This entailed eliminating biased data from the sample set while demonstrating heterogeneity in the forest plot.

Validation of the sensitivity and robustness of the variables is a necessary factor for the reliability of the receptor model. The sensitive factor and root-mean-square algorithm were used in the sensitivity analysis in this study, which can evaluate the influence of parameters

on the model output, as expressed in formula 2.

$$\delta_j = \sqrt{\frac{1}{n} \sum_{j=1}^n \left(\frac{\Delta y_j x_j}{\Delta x_j y_j} \right)^2} \quad (2)$$

Where δ_j is the root-mean-square sensitivity coefficient; vector y_j ($j = 1, 2, \dots, n$) are the output variables; the vector x_j ($j = 1, 2, \dots, n$) represents the corresponding input variables, namely, the model parameters, with 10% of their initial value modified in each analysis; and n is the number of output variables.

To evaluate the robustness, the variable substitution method is adopted, that is, the independent variable in the formula is replaced with another strongly correlated indicator. If the R2 of the linear fitting consequence does not decrease significantly, it indicates that the variable is robust. All datasets will be utilized as fitting data for the receptor model, and the prediction accuracy of the model will be assessed. Additionally, the relative deviation between the model values and the fitting values will be evaluated. Owing to the guidance of the PCA and the scientific establishment of the background value (initial field), the receptor model is able to explain a significant portion of the numerical variation. It can also evaluate the weight of the influencing factors simply and straightforwardly, leading to mechanistic conclusions. To evaluate and improve the predictive capability of receptor models, two models, XGBoost and RandomForest, were introduced to enhance linear regression.

XGBoost is a gradient-boosting algorithm that utilizes regularization, feature splitting, and parallel computation to enhance the model's generalization capability and mitigate the risk of overfitting. RandomForest, on the other hand, is an ensemble learning method comprising multiple decision trees. Each decision tree is trained on a randomly chosen subset of features, and the predictions are made using techniques like voting or averaging. These two models, XGBoost and RandomForest, will be employed to refine and enhance the receptor model by leveraging their improved regression fitting abilities. The accuracy of the aforementioned approach will serve as a control group for evaluating the model's prediction accuracy.

Data availability

All data used in this study are freely available online. TMs and nutrients datasets from <http://gdee.gd.gov.cn/gkmlpt/index>. The CMIP6 model simulations are from <https://esgf-node.llnl.gov/search/cmip6/>. None of them requires account login. The prediction data generated in this study can be found in Supplementary Information Part B. This part is also stored on figshare (<https://doi.org/10.6084/m9.figshare.28282469>)⁴¹. Source data are provided with this paper.

Code availability

Source code for an efficient implementation of the proposed procedure is available at figshare (<https://doi.org/10.6084/m9.figshare.28452593>)⁴².

References

- Walsh, J. J. Importance of continental margins in the marine biogeochemical cycling of carbon and nitrogen. *Nature* **350**, 53–55 (1991).
- Mackenzie, F. T., Lerman, A. & Ver, L. M. B. Role of the continental margin in the global carbon balance during the past three centuries. *Geology* **26**, 423–426 (1998).
- Bauer, J. E. et al. The changing carbon cycle of the coastal ocean. *Nature* **504**, 61–70 (2013).
- Gruber, N. Carbon at the coastal interface. *Nature* **517**, 148–149 (2015).
- Payea, M. J. et al. Senescence suppresses the integrated stress response and activates a stress-remodeled secretory phenotype. *Mol. Cell* **84**, 4454–4469 (2024).
- Zhang, Z. et al. Mechanisms underlying the alleviated cadmium toxicity in marine diatoms adapted to ocean acidification. *J. Hazard. Mater.* **463**, 132804 (2024).
- Beiras, R. *Marine pollution: sources, fate and effects of pollutants in coastal ecosystems*. (Elsevier, 2018).
- Lotze, H. K. et al. Depletion, degradation, and recovery potential of estuaries and coastal seas. *Science* **312**, 1806–1809 (2006).
- Gao, X., Zhou, F. & Chen, C. T. A. Pollution status of the Bohai Sea: An overview of the environmental quality assessment related trace metals. *Environ. Int.* **62**, 12–30 (2014).
- Liu, Y. et al. Distribution, source and risk assessment of heavy metals in the seawater, sediments, and organisms of the Daya Bay, China. *Mar. Pollut. Bull.* **174**, 113297 (2022).
- Guan, X. et al. Probing the national development from heavy metals contamination in river sediments. *J. Clean Prod.* **419**, 138164 (2023).
- Biguino, B., Haigh, I. D., Dias, J. M. & Brito, A. C. Climate change in estuarine systems: Patterns and gaps using a meta-analysis approach. *Sci. Total Environ.* **858**, 159742 (2023).
- Ji, C. et al. Analyzing the variation of the precipitation of coastal areas of eastern China and its association with sea surface temperature (SST) of other seas. *Atmos. Res.* **219**, 114–122 (2019).
- Zhang, L. et al. Spatial and seasonal characteristics of dissolved heavy metals in the east and west Guangdong coastal waters, South China. *Mar. Pollut. Bull.* **95**, 419–426 (2015).
- Zhai, F. G. et al. Satellite-observed interannual variations in sea surface chlorophyll-a concentration in the yellow sea over the past two decades. *J. Geophys. Res.-Oceans* **128**, <https://doi.org/10.1029/2022jc019528> (2023).
- Ardelan, M. V., Steinnes, E., Lierhagen, S. & Linde, S. O. Effects of experimental CO₂ leakage on solubility and transport of seven trace metals in seawater and sediment. *Sci. Total Environ.* **407**, 6255–6266 (2009).
- Boyd, P. W., Ellwood, M. J., Tagliabue, A. & Twining, B. S. Biotic and abiotic retention, recycling and remineralization of metals in the ocean. *Nat. Geosci.* **10**, 167–173 (2017).
- Ratnarajah, L. et al. Monitoring and modelling marine zooplankton in a changing climate. *Nat. Commun.* **14**, 564 (2023).
- Wang, H. et al. Spatiotemporal redox heterogeneity and transient marine shelf oxygenation in the Mesoproterozoic ocean. *Geochim. Cosmochim. Acta* **270**, 201–217 (2020).
- Westberry, T. K. et al. Atmospheric nourishment of global ocean ecosystems. *Science* **380**, 515–519 (2023).
- Yu, G. et al. Stabilization of atmospheric nitrogen deposition in China over the past decade. *Nat. Geosci.* **12**, 424–429 (2019).
- Paerl, H. W. Coastal eutrophication and harmful algal blooms: Importance of atmospheric deposition and groundwater as “new” nitrogen and other nutrient sources. *Limnol. Oceanogr.* **42**, 1154–1165 (1997).
- Jiskra, M. et al. Mercury stable isotopes constrain atmospheric sources to the ocean. *Nature* **597**, 678–682 (2021).
- Howarth, R. et al. Coupled biogeochemical cycles: eutrophication and hypoxia in temperate estuaries and coastal marine ecosystems. *Front. Ecol. Environ.* **9**, 18–26 (2011).
- Liu, M., Chen, J. B., Sun, X. S., Hu, Z. Z. & Fan, D. J. Accumulation and transformation of heavy metals in surface sediments from the Yangtze River estuary to the East China Sea shelf. *Environ. Pollut.* **245**, 111–121 (2019).
- Dai, Y. H. et al. Coastal phytoplankton blooms expand and intensify in the 21st century. *Nature* **615**, 280 (2023).
- Zhang, C. et al. Occurrence and distribution of microplastics in commercial fishes from estuarine areas of Guangdong, South China. *Chemosphere* **260**, 127656 (2020).

28. EPA, U. E. P. A. CMC, acute (criterion maximum concentration in freshwater for National Recommended Aquatic Life Criteria). Washington, DC; (2009).
29. Xu, H. et al. Source contribution analysis of mercury deposition using an enhanced CALPUFF-Hg in the central Pearl River Delta, China. *Environ. Pollut.* **250**, 1032–1043 (2019).
30. Zhong, Z., Li, J., Ma, Y. & Yang, Y. The adsorption mechanism of heavy metals from coal combustion by modified kaolin: Experimental and theoretical studies. *J. Hazard. Mater.* **418**, 126256 (2021).
31. Wang, J., Beusen, A. H. W., Liu, X. & Bouwman, A. F. Aquaculture Production is a Large, Spatially Concentrated Source of Nutrients in Chinese Freshwater and Coastal Seas. *Environ. Sci. Technol.* **54**, 1464–1474 (2020).
32. Ge, C., Chai, Y., Wang, H. & Kan, M. Ocean acidification: One potential driver of phosphorus eutrophication. *Mar. Pollut. Bull.* **115**, 149–153 (2017).
33. Kessouri, F. et al. Coastal eutrophication drives acidification, oxygen loss, and ecosystem change in a major oceanic upwelling system. *Proc. Natl Acad. Sci.* **118**, e2018856118 (2021).
34. Maneux, E. et al. Temporal patterns of the wet deposition of Zn, Cu, Ni, Cd and Pb: The Arcachon Lagoon (France). *Water, Air, Soil Pollut.* **114**, 95–120 (1999).
35. Scholz, F., McManus, J., Mix, A. C., Hensen, C. & Schneider, R. R. The impact of ocean deoxygenation on iron release from continental margin sediments. *Nat. Geosci.* **7**, 433–437 (2014).
36. Wei, G. et al. BOD/COD ratio as a probing index in the O/H/O process for coking wastewater treatment. *Chem. Eng. J.* **466**, 143257 (2023).
37. Taucher, J. et al. Changing carbon-to-nitrogen ratios of organic-matter export under ocean acidification. *Nat. Clim. Chang.* **11**, 52–57 (2021).
38. Zhou, J. et al. Effects of acidification on nitrification and associated nitrous oxide emission in estuarine and coastal waters. *Nat. Commun.* **14**, 1380 (2023).
39. Guangdong Provincial Department of Ecological Environment. Monitoring information of rivers entering the sea in Guangdong Province. p.3. 2022-12-8. Available from: <http://gdee.gd.gov.cn/zdgg/index.html>.
40. Eyring, V. et al. Overview of the coupled model intercomparison project phase 6 (CMIP6) experimental design and organization. *Geosci. Model Dev.* **9**, 1937–1958 (2016).
41. Guan, X. H. Model dataset, including the sources and output results. figshare. Dataset. <https://doi.org/10.6084/m9.figshare.28282469.v1> (2025).
42. Guan, X. H. The code used for model training. figshare. Software. <https://doi.org/10.6084/m9.figshare.28452593.v1> (2025).

Acknowledgements

This work was supported by the National Natural Science Foundation of China (No. U1901218 and No. 42277379), and the sponsor is C. H. Wei. Thanks to Professor X. Huang for the language help.

Author contributions

X.H.G. and H.H. are the core researchers and writers of the paper. They have made major contributions to data analysis and model analysis. X.Q.C. and X.K. provided the sources and analysis of chemical data. H.Z. and A.C.C. provided the sources and analysis of biological data. H.Z.W. and G.L.Q. respectively provided the research experimental platform and organized onsite sampling, and participated in the discussion and revision of the paper. C.H.W. is the project leader and has contributed to the design of the research plan, the writing content, and the positioning of viewpoints.

Competing interests

The authors declare no competing interests.

Additional information

Supplementary information The online version contains supplementary material available at <https://doi.org/10.1038/s41467-025-57913-4>.

Correspondence and requests for materials should be addressed to Chaohai Wei.

Peer review information *Nature Communications* thanks the anonymous reviewer(s) for their contribution to the peer review of this work. A peer review file is available.

Reprints and permissions information is available at <http://www.nature.com/reprints>

Publisher's note Springer Nature remains neutral with regard to jurisdictional claims in published maps and institutional affiliations.

Open Access This article is licensed under a Creative Commons Attribution-NonCommercial-NoDerivatives 4.0 International License, which permits any non-commercial use, sharing, distribution and reproduction in any medium or format, as long as you give appropriate credit to the original author(s) and the source, provide a link to the Creative Commons licence, and indicate if you modified the licensed material. You do not have permission under this licence to share adapted material derived from this article or parts of it. The images or other third party material in this article are included in the article's Creative Commons licence, unless indicated otherwise in a credit line to the material. If material is not included in the article's Creative Commons licence and your intended use is not permitted by statutory regulation or exceeds the permitted use, you will need to obtain permission directly from the copyright holder. To view a copy of this licence, visit <http://creativecommons.org/licenses/by-nc-nd/4.0/>.

© The Author(s) 2025